

Linear vs Nonlinear Extreme Learning Machine for Spectral-Spatial Classification of Hyperspectral Image

Faxian Cao¹, Zhijing Yang^{1*}, Jinchang Ren², Mengying Jiang¹, Wing-Kuen Ling¹

¹School of Information Engineering, Guangdong University of Technology, Guangzhou, 510006, China

²Department of Electronic and Electrical Engineering, University of Strathclyde, Glasgow, G1 1XW, UK

*Email: yzhj@gdut.edu.cn

Abstract— As a new machine learning approach, extreme learning machine (ELM) has received wide attentions due to its good performances. However, when applied to the hyperspectral image (HSI) classification, the recognition rate is low. That is because ELM does not use the spatial information that is very important for HSI classification. In view of this, this paper proposes a new framework for spectral-spatial classification of HSI by combining ELM with loopy belief propagation (LBP). The original ELM is linear, and the nonlinear ELMs (or Kernel ELMs) are the improvement of linear ELM (LELM). However, based on lots of experiments and analysis, we found out that the LELM is a better choice than nonlinear ELM for spectral-spatial classification of HSI. Furthermore, we exploit the marginal probability distribution that uses the whole information in the HSI and learn such distribution using LBP. The proposed method not only reduces the computation time, but also greatly improves the accuracy of classification. The experimental results in the well-known HSI data sets, Indian Pines and Pavia University, demonstrate the good performances of the proposed method.

Index Terms—Hyperspectral image (HSI) classification, extreme learning machine (ELM), discriminative random field (DRF), loopy belief propagation (LBP).

I. INTRODUCTION

Classification is the basic research and an important mean of obtaining information from hyperspectral images (HSI). The main goal of HSI classification is to divide each pixel in the image into different classes according to the spectral information and the spatial information. Each pixel of HSI has many spectral features. Therefore, it is difficult to classify HSI with limited samples and high spectral resolution of each pixel, which is a challenging problem for HSI classification. There are some typical algorithms for HSI images classification, such as support vector machine (SVM) [2], sparse multinomial logistic regression (SMLR) [12], and so on. Many techniques have been proposed for feature extraction and dimensionality reduction [3], [4], such as singular spectrum analysis (SSA) [5]-[8], principal component analysis (PCA) [9], [10] and spectral-spatial classification methods [11], [12] and so on. However, there are still many challenges in HSI classification, for example, the data structure of each pixel in the HSI data is very complex, and each pixel of HSI data sets has very large dimensions. Therefore, it is very difficult to not only reduce time-consuming for classification, but also

achieve high accuracy for classification with little training samples.

As a new machine learning approach that has single-hidden layer feedforward neural network, ELM has received wide attentions due to its good performances. It has been proved to be a promising algorithm in pattern recognition fields [17]-[21]. Compared with support vector machine and other state-of-the-art algorithms, ELM has the following advantages [21]: very simple structure and higher generalization, high computational efficiency without tuning additional parameters. The original ELM is a linear operation, so we call it linear ELM (LELM). Although it has the above advantages, the classification accuracy is not very high when applied to hyperspectral images. Kernel ELM (KELM) [22] and sparse ELM [23] are the improvements of LELM and achieve better classification results for pattern recognition. Compared with ELM, KELM had solved the problem that randomly generating weights and biases of hidden layers which may cause ill-posed problems. The accuracy of KELM is improved but still not high enough when applied to the classification of HSI. So it is a critical problem that not only maintaining the property of fast speed, but also improving the classification accuracy for HSI classification with ELM. The main reason that ELM and KELM cannot achieve high accuracy of classification is that they just make use of spectral information of HSI, without the spatial information of HSI. The spatial information which reflects the local property of HSI data sets is very important for classification.

To improve the performance of ELM for HSI classification, Loopy belief propagation (LBP) algorithm is used here [27], [28]. It is a conditional probability model, which can be considered as a generalization of the Markov chain and can effectively describe the correlation of all the nodes in the field. It is based on the Markov random field (MRF) which assumes that the neighboring pixels likely belong to the same class [24]-[26]. The principle of LBP for classification is to calculate the marginal probability based on the characteristics of the samples. Since the KELM is the improvement of ELM, KELM and MRF have been combined for spectral and spatial classification of HSI [16]. It can improve the recognition result of KELM to some extent. However, based on lots of experiments and analysis, we found out that the linear ELM is a bet-

ter choice than KELM for spectral-spatial classification of HSI.

LELM is a type of linear operation, so its final mapping results will not change the characteristics of pixels in HSI. Nevertheless, KELM is a type of nonlinear operation, so called NLELM, and its final mapping results will disturb the features of pixels in the same class. If we use the output of NLELM as the input of MRF or LBP, the structure of NLELM will seriously disturb the original information of HSI. Then it cannot fully utilize the spectral information and spatial information of HSI and will cause the classification accuracy relative low. For example, the NLELM and MRF are combined for classification of HSI in [16], called NLELM-MRF. NLELM disturbs the features of pixels in the same class and causes the classification accuracy relative low. The same problem happened in [29]-[31], where the spectral information of the HSI is extracted by kernel sparse MLR (KSMLR) before using spatial information to classify HSI with MRF. The sparse MLR can be kernel (KSMLR) or non-kernel (SMLR) forms. The kernel form is a type of nonlinear operation, so it will disturb the features of pixels in HSI, and cause the classification results relative low. The non-kernel of SMLR will also disturb the features of pixels in HSI, and this is because the regressor of SMLR need to iterations. Hence, the final output of SMLR will disturb the salient features of HSI. In summary, we should not disturb the features of pixels in HSI before using spatial information for improving the classification accuracies of HSI. Hereby, LELM is used here with LBP for spectral-spatial classification of HSI to achieve high classification accuracy.

As mentioned above, LBP algorithm is based on the MRF. The LBP uses the information of the node and the node to transmit information to update the current MRF marking state. It is a kind of approximate calculation based on MRF. This algorithm is an iterative method, which can solve the problem of probabilistic inference in probabilistic graphical models. After many iterations of probability, the belief of all the nodes is no longer changed. Then the LBP algorithm can converge to its optimal solution. Since the pixels of HSI that need to be classified are just a part of HSI, it means that not all the pixels in HSI need to be classified. If we use LBP to classify HSI directly, it may cause ill-posed problems. In view of this, we make some improvement of LBP for HSI classification. The pixels of background of HSI are ignored in LBP. The proposed framework will fully make use of spectral and spatial information to improve the classification accuracy dramatically. Experiment results demonstrate the better performance compared with other state-of-the-art at same situation.

The remaining of this paper is divided into the following sections: Section II gives the detail of the proposed method. Section III shows the extensive experimental results and analysis. Conclusions are summarized in Section IV.

II. PROPOSED METHOD BASED ON LELM AND LBP

A. Normalization

Let $X \equiv (X_1, X_2, \dots, X_N) \in R^{N \times d}$ be HSI data, which has N samples and each sample has d feature. Normalization is a preprocessing process and has a great influence on the subsequent classification of data. Based on lots of experiments, we choose the stable normalization method as follows:

$$x_{ij} = X_{ij} / \max(X) \quad (1)$$

where X_{ij} is any pixel value of the HSI data, $\max()$ is the largest value of all the data in the HSI.

B. Linear ELM

For convenient, let $x \equiv (x_1, x_2, \dots, x_N) \in R^{N \times d}$ be the HSI data after normalization, $y \equiv (y_1, y_2, \dots, y_N) \in R^{N \times M}$ denotes the class labels. As a new learning algorithm, ELM [17] is a single layer feedforward neural network and it can be modeled as:

$$\sum_{m=1}^L \sum_{j=1}^N \beta_{jm} g_{jm}(w_i^T x_i + b_i) = y^T \quad (2)$$

where $w_i = (w_{i1}, w_{i2}, \dots, w_{id})^T$ is the weight vector which connects the input layer with hidden layer of i-th sample. b_i is the bias connecting input layer with hidden layer of i-th sample and β_j is the output weight vector of i-th sample. T is the transpose operation and $g()$ is the activation function of the hidden layer. The main steps of classification with ELM are as follows:

Step1: Assign random input w_i and bias b_i , $i = 1, 2, \dots, N$ for the input layer.

Step2: Calculate the output matrix of hidden layer G as:

$$G(w_1, w_2, \dots, w_N; x_1, x_2, \dots, x_N; b_1, b_2, \dots, b_N) = \begin{bmatrix} g_{11}(w_{11}x_{11} + b_{11}) & \dots & g_{1L}(w_{1L}x_{1L} + b_{1L}) \\ \dots & \dots & \dots \\ g_{N1}(w_{N1}x_{N1} + b_{N1}) & \dots & g_{NL}(w_{NL}x_{NL} + b_{NL}) \end{bmatrix} \quad (3)$$

Step3: Calculate the output matrix β :

$$\beta = G^T y \quad (4)$$

where

$$\beta = [\beta_1, \dots, \beta_L]_{L \times M}^T$$

and \dagger is the Moore-Penrose generalized inverse of hidden layer matrix.

Step4: The result of the final classification of ELM can be expressed by the following equation:

$$f(x) = G * \beta \quad (5)$$

The execution time of ELM can be greatly reduced because the input weight and bias of ELM are randomly generated, so the output weight can be computed as $\beta = G^T * y$. Any piecewise continual function can be used as the hidden layer activation function. Obviously, ELM is a lineal operation.

C. Nonlinear ELM

The classification problem for NLELM [22] can be formulated as:

$$\begin{aligned} \text{Minimize: } L_{NLELM} &= \frac{1}{2} \|\beta\|^2 + C \frac{1}{2} \sum_{i=1}^N \|\varepsilon_i\|^2 \\ \text{subject to: } h(x_i)\beta &= t_i^T - \varepsilon_i^T, i=1, \dots, N \end{aligned} \quad (6)$$

where $\varepsilon_i = [\varepsilon_{i,1}, \dots, \varepsilon_{i,M}]$ is the error vector of the M output nodes relative to the sample x_i . Based on

the KKT theorem, equation (6) is equivalent to solve the following dual optimization problem:

$$L_{NLELM} = \frac{1}{2} \|\beta\|^2 + C \frac{1}{2} \sum_{i=1}^N \|\varepsilon_i\|^2 - \sum_{i=1}^N \sum_{j=1}^M \alpha_{i,j} (h(x_i) \beta_j - t_i^T + \varepsilon_i^T) \quad (7)$$

where β_j is the vector of weight between hidden layer and output layer. $\alpha_{i,j}$ is the Lagrange multiplier. Based on the KKT theorem, we can conclude that:

$$\frac{\partial L_{NLELM}}{\partial \beta_j} = 0 \rightarrow \beta = H^T \alpha \quad (8)$$

$$\frac{\partial L_{NLELM}}{\partial \varepsilon_i} = 0 \rightarrow \alpha_i = C \varepsilon_i \quad (9)$$

$$\frac{\partial L_{NLELM}}{\partial \alpha_i} = 0 \rightarrow h(x_i) \beta_j - t_i^T + \varepsilon_i^T \quad (10)$$

where $i=1, \dots, N$, $\alpha_i = [\alpha_{i,1}, \alpha_{i,2}, \dots, \alpha_{i,M}]^T$ and $\alpha = [\alpha_1, \alpha_2, \dots, \alpha_N]^T$. Now the output weight β can be formulated as:

$$\beta = (\frac{I}{C} + H^T H)^{-1} H^T y. \quad (11)$$

The hidden neurons are unknown. Any kernel satisfying the Mercer's conditions can be used:

$$\Omega_{KELM} = H H^T:$$

$$\Omega_{KELM}(x_i, x_j) h(x_i) h(x_j)^T = K(x_i, x_j) \quad (12)$$

In general, the Gaussian kernel is chosen:

$$K_{NLELM}(x_i, x_j) = \exp\left(-\frac{\|x_i - x_j\|^2}{2 * \sigma_{NLELM}^2}\right) \quad (13)$$

Then the NLELM can be constructed using only the kernel function.

Suppose that w is the feature-weight vector corresponding to class y_i . Giving the sample x_i that belongs to class y_i , according to the SMLR model [28] [31], the probability $p(y_i/x_i)$ can be formulated as follows:

$$p(y_i/x_i, w) = \exp(w^{(k)T} h(x_i)) / \sum_{j=1}^K \exp(w^{(j)T} h(x_i)) \quad (14)$$

where $h(x) = [h_1(x), \dots, h_l(x)]$ is a vector of l fixed functions of the input, $w = [w^{(1)T}, \dots, w^{(k)T}]$, K is the total number of classes.

The general prior of w can be modeled as Laplacian density [30]:

$$p(w) \propto \exp(-\lambda \|w\|_1) \quad (15)$$

where λ is the regularization parameter used to control the sparsity of w . The maximum a posterior (MAP) estimation of the regressors can be formulated as:

$$w^* = \arg \max_w l(w) + \log p(w) \quad (16)$$

where $l(w)$ is the log-likelihood function and can be written as :

$$l(w) = \log \prod_i p(y_i/x_i, w) \quad (17)$$

In general, the $h(x)$ in (14) is the kernel that $h(x) = [1, K(x, x_1), K(x, x_2), \dots, K(x, x_n)]^T$ and $K(\dots)$ can be any symmetric kernel function, where the Gaussian RBF kernel function is used in this paper:

$$K_{KSMLR}(x_i, x_j) = \exp\left(-\frac{\|x_i - x_j\|^2}{2 * \sigma_{KSMLR}^2}\right) \quad (18)$$

It can be seen that w in (15) need to be computed by iterations. So the final result of (14) may disturb the features of the pixels, and its classification accuracy combining spatial information will not be good.

There is no doubt that NLELM and KSMLR can achieve higher classification accuracy than LELM if we just consider the spectral information. As mentioned above, LELM is a linear operation for classification, and NLELM and KSMLR are nonlinear operations. So their classification performances are better than the performance of LELM when just considering spectral information. The nonlinear operation is better than the linear operation in some aspects. However, the nonlinear operation will disturb the original features of the HSI data. If the subsequent classification needs to use the spatial information for classification, it will cause the classification accuracy relative low. So we will choose the LELM with LBP for spectral-spatial classification of HSI.

C. Using Spatial Information to Improve the Classification Accuracy Based on LBP

To further extract the spatial information, the output of LELM is used as the input of LBP. The posterior density $p(y/x)$ is obtained according to the feature x that it is the output of LELM. We adopt the discriminative random field (DRF) [32] as:

$$P(y/x) = \frac{1}{Z(x)} \exp(\sum \log p(y_i/x_i) + \sum \log p(y_i, y_j)) \quad (19)$$

where $Z(x)$ is the partition function. The term $\log p(y_i/x_i)$ is the association potential that model the likelihood of label y_i given the feature x_i , and $\log p(y_i, y_j)$ is the interaction potential.

We adopt an isotropic MLL prior to the model image of class label y in order to use the spatial information of HSI. This prior belongs to the MRF class and encourages piecewise smooth segmentations. It tends to produce solutions that the adjacent pixels are likely to belong to the same class [12]. The MLL prior has been widely used in image segmentation problems [33]-[36] and is a generalization of the Ising model [37]-[38]. It can be formulated as:

$$p(y) = \frac{1}{Z} \exp^{\mu \sum \delta(y_i, y_j)} \quad (20)$$

where μ is a tunable parameter controlling the degree of smoothness, Z is a normalization constant for the density, $\delta(y)$ is the unit impulse function. The pairwise interaction term $\delta(y_i, y_j)$ assigns high probability to the neighborhood labels.

Maximum a posterior (MAP) estimate will minimize the Bayesian risk associated to the zero-one loss function [11]. The MAP estimate of y can be given by:

$$y^* = \arg \min_y \sum -\log(y_i/x_i) - \mu \sum \delta(y_i - y_j) \quad (21)$$

This is a combinatorial optimization problem having pairwise interaction terms. An alternative MAP solution is the MAP marginal (MAM) solution, which minimizes the Bayesian risk associated to the zero-one loss function. The MAM estimation of label y_i can be formulated as:

$$y_i^* = \arg \max_{y_i} q(y_i/x) \quad (22)$$

where $q(y_i/x)$ is the marginal density of $p(y/x)$ respect to y_i . The computation of marginal density

of $p(y/x)$ in (19) is difficult [11]. Since the LBP is an efficient approach to estimate Bayesian beliefs [26] in graphical model, we will use LBP to estimate the MAM solution and let the output of LELM y_{LELM}^* be the input of LBP.

Fig.1 is a graphical example of MRF, where each node represents a random variable or a hidden node, and the class label y_i here is associated with each input feature x_i . In the graphical example of MRF, $\psi_{ij}(y_i, y_j) = p(y_i, y_j)$ denotes the interaction potential that penalizes the dissimilar pair of neighboring label. $\varphi_i(y_i, x_i) = p(y_i/x_i)$ stands for the association potential of label y_i respect to evidence. Suppose we observe some information about x_i . Each node has the state value y_i , and the observation value x_i . $\varphi_i(y_i, x_i)$ reflects the existence of statistical dependence. $\psi_{ij}(y_i, y_j)$ is the potential energy between adjacent neighbor nodes, and reflects the compatibility between the node variables y_i and y_j .

Fig.2 provides a graphical example of an undirected network. Since LBP is an iterative algorithm, at the iteration t , the message sent from node i to its neighbor node $j \in N(i)$ can be given by the following equation :

$$m_{ij}^t(y_j) = \frac{1}{Z} \sum_{y_i} \psi(y_i, y_j) \varphi(y_i, x_i) \prod_{k \in N(i) \setminus \{j\}} m_{ki}^{t-1}(y_i) \quad (23)$$

where Z is a normalization constant.

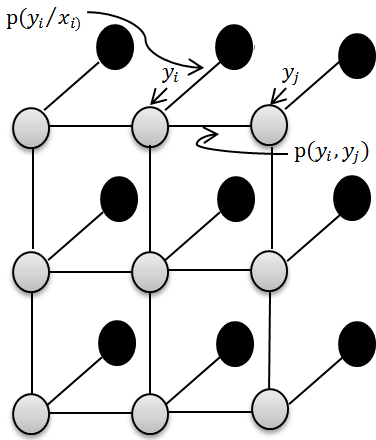


Fig.1. Graph example of MRF.

Assume that $b_i^t(y_i)$ is the belief of node i at the iteration t , so $b_i^t(y_i)$ can be presented by the following equation:

$$b_i^t(y_i = k) = q(y_i = k/x) = \varphi(y_i = k) \prod_{j \in N(i)} m_{ji}^t(y_i = k) \quad (24)$$

Finally, we can estimate the final solution using maximize of the posterior marginal for node i :

$$\hat{y}_i = \arg \max_{y_i} q(y_i/x) = \arg \max_{y_i} b_i^t(y_i) \quad (25)$$

As we know, not all the pixels, but only part of the HSI needs to be classified. For instance, the size of HSI data set of Indian Pines is $145 \times 145 \times 200$, so the size of ground-truth is 145×145 . But only 10366 out of 21025 pixels need to be classified. It may cause ill-posed problems if we use LBP directly. In view of this, we do some improvement of LBP (ILBP) in order to solve this problem, where we discard the pixel that belongs to the background, i.e. we just consider the pixels that need to be classified. The proposed method is summarized in Algorithm 1.

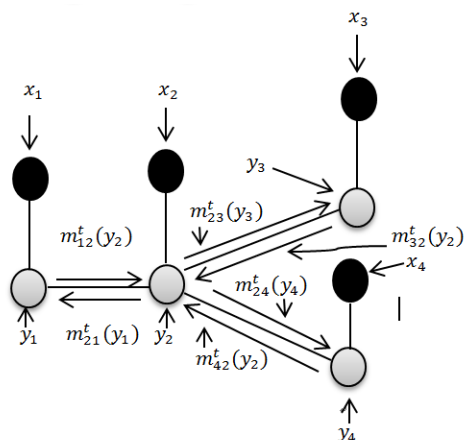


Fig.2. Message passing of LBP at iteration t.

Algorithm 1: Spectral-Spatial Classification for HSI Based on LELM and ILBP

Input: X: the HSI image; X1: training samples; X2: test samples; Y1: The desired output of training sample; Y2: The desired output of test sample; L: number of hidden node of ELM; g(): activation function of hidden layer of ELM.

(1) **Normalization:** Let $X1^* = X1/\max(X)$, $X2^* = X2/\max(X)$.

(2) **LELM training:**

Step 1: Randomly generate the input weights, w_i , and bias, b_i .

Step 2: Calculate the hidden layer of output matrix:

$$G1 = g(w_i^T * X1^* + b_i)$$

Step3: Calculate the output weight:

$$\beta = G^T * Y1$$

Output of LELM: Calculating the hidden layer matrix of the test samples: $G2 = g(w_i^T * X2^* + b_i)$.

Get the output result of LELM: $Y_{ELM} = G2 * \beta$.

(3) **Spatial Classification by ILBP:**

Step1: Find the index of adjacent pixels of training samples and test samples and eliminate the pixels of background.

Step 2: Calculate the marginal of MPA as follows:

For $t=1$: time of iterations

For $j=1$: number of pixels

If $j \sim =$ test sample

Don't calculate the marginal of MAM.

Else

Calculate the marginal of MAM:

$$m_{ij}^t(y_j) = \frac{1}{Z} \sum_{y_i} \psi(y_i, y_j) \phi(y_i, x_i) \prod_{k \in N(i) \setminus \{j\}} m_{ki}^{t-1}(y_i)$$

Then the belief of node i at the iteration t can be represented as:

$$b_i^t(y_i = k) = q(y_i = k/x) = \phi(y_i = k) \prod_{j \in N(i)} m_{ji}^t(y_i = k)$$

End

End

The final solution for node i can be obtained by maximizing the posterior marginal:

$$y_i^* = \arg \max_{y_i} q(y_i/x) = \arg \max_{y_i} b_i^t(y_i).$$

III. EXPERIMENTS AND ANALYSIS

A. HSI Data Set

(1) Indian Pines: The Indian Pines HSI data set was the urban image collected in June 1992 by the AVIRIS sensors over the Indian Pines region. The data set has 145×145 pixels which each has 200 spectral bands after removing 20 water absorption bands ranging from 0.2 to $2.4 \mu\text{m}$. There are totally 16 classes. The number of training and test samples of each class is shown in Table 1.

(2) Pavia University: The Pavia university HSI data set was acquired in 2001 by the Reflective Optics System Imaging Spectrometer, flown over city of Pavia Italy. The sensor collects HSI data set in 115 spectral bands ranging from 0.43 to $0.86 \mu\text{m}$ with a spatial resolution of 1.3m/pixel. 103 bands were selected for experiment after removing 12 noisiest bands. The image scene contains 610×340 pixels and there are totally 9 classes. The number of training sample and test sample is shown in Table 1.

B. Parameter Settings

All the experimental results are assessed by the overall accuracier (OA), averse accuracies (AA) and kappa stastistic (k) [31]. In order to avoid the influences induced by the selection of training

samples, ten independent Monte Karlo runs are perfomed and OA, AA, k are all averaged by ten runs.

In order to compare the performance of the proposed method with other classifiers and avoid the impact induced by the parameter setting, we give the parameter settings in the experiments. The kernel function is the Gaussian RBF with σ_{KSMLR} in (18). According to [29], λ in (15) is set to 10^{-2} , σ_{KSMLR} is set to 0.85 for Indian Pines, and 0.35 for the Pavia University (It should be noting that the SMLR and KSMLR are multinomial logistic regression (MLR) via variable splitting and augmented Lagrangian (LORSAL) [39], which can decrease the computation time of SMLR and KSMLR [40]). The cost function $C = 2^b$ of NLELN is in the range of $= [0, 1, 2, \dots, 10]$ and the kernel function is also Gaussian RBF in (12) with $\sigma_{NLELM} = 2^\tau$, $\tau = \{-9, -8, \dots, 0, \dots, 8, 9\}$, and the parameters is set as $b=9$, $\tau = -1$, it should be noting that the parameters setting of NLELM is the best parameters for NLELM by our experiments. For LELM, hidden node L in (3) is a very important parameter and we will evaluate the impact in the next subsection. The μ in (21) is a tunable parameter controlling the degree of smoothness, which is set as $\mu = 20$ for Indian Pines and

Pavia University. We will further evaluate the impact on the proposed approach in the next subsection. It should be noting that the output of LELM and NLELM are probability output. All the experiments are conducted in MATLAB R2016b on a computer with 3.50GHz CPU and 32.0G RAM

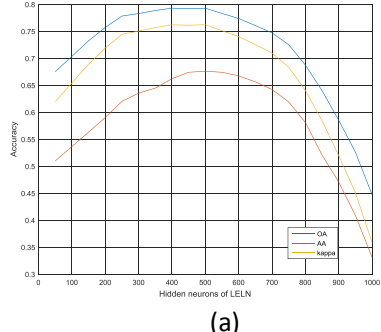
C. Impact of parameters L and μ

In this subsection, we will evaluate the impact of the hidden neurons of LELM, L , and the smoothness parameter, μ , using the Indian Pines and Pavia University date sets. Table 1 displays the numbers of training samples and test samples.

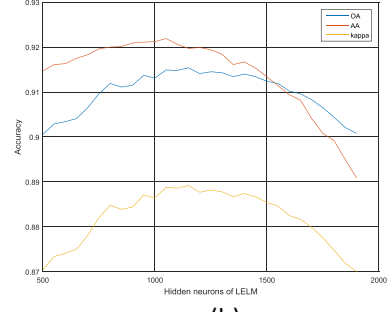
Fig. 4 shows the OA, AA and kappa statistic results as a function of variable L with the training samples of 1043 and 3921 in the Indian Pines and Pavia University, respectively (about 9% and 10% of the available sample, respectively). The training samples are randomly selected from each class in

each Monte Carlo Run. From Fig. 4 (a) and (b), we can see that the classification accuracies of LELM indeed depend on the hidden neurons, so we should choose the best hidden neurons for LELM in order to improve the classification performance in the sequential spatial information classification. We can see that the best hidden neurons of LELM for Indian Pines is about 450 and the best hidden neurons of LELM for Pavia University is about 1050. Therefore, we will use hidden neurons 450 for Indian Pines and 1050 for Pavia University.

Fig. 5 (a) and (b) shows the OA, AA and kappa statistic as a function of variable μ , we can see that the performance of the proposed framework depend on the smoothness parameter. However, the classification performance is very stable and keeps the high classification accuracy as μ is increasing. This also demonstrates the proposed framework is very robust.

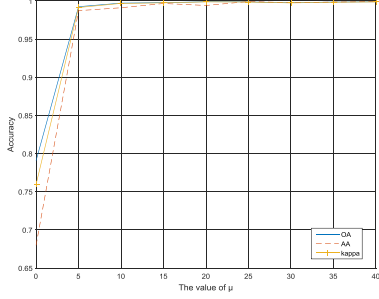


(a)

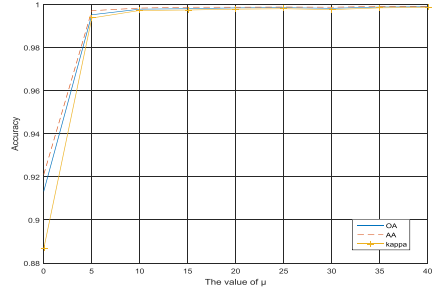


(b)

Fig. 4 The impact of hidden neurons of ELM in (a) the Indian Pines and (b) Pavia University



(a)



(b)

Fig. 5 The impact of sparseness parameters μ in (a) the Indian Pines and (b) Pavia University

Table 1. The training sample and test samples of Indian Pines and Pavia University

Indian Pines						Pavia University		
Class	Train	Test	Class	Train	Test	Class	Train	Test
Alfalfa	6	54	Oats	2	20	Asphalt	548	6631
Corn-no till	144	1434	Soybeans-no till	97	968	Meadows	548	18649
Corn-min till	84	834	Soybeans-min till	247	2468	Gravel	392	2099
Corn	24	234	Soybeans-clean till	62	614	Trees	524	3064
Grass/pasture	50	497	Wheat	22	212	Metal sheets	265	1345
Grass/tree	75	747	Woods	130	1294	Bare soil	532	5029
Grass/pasture-mowed	3	26	Bldg-grass-tree-drives	38	380	Bitumen	375	1330
Hay-windrowed	49	489	Stone-steel towers	10	95	Bricks	514	3682
Total	1043	10366				Shadows	231	947
						Total	3921	42776

D. The Experiment Results and Analysis of Two HSI Data Sets

In this subsection, we will evaluate the HSI classification accuracy of the proposed method in two HSI data sets by comparing other state-of-the-art methods of HSI classification, including sparse multinomial logistic regression (SMLR) [12], kernel sparse multinomial logistic regression (KSMLR) [30], nonlinear ELM (NLELM) [22], linear ELM (LELM) [21], SMLR+LBP, KSMLR+LBP, and NLELM+LBP. For the normalization method, we all use *Max* method in equation (1) for all algorithms. Table 1 shows the numbers of training sample and testing sample of Indian Pines and Pavia University.

For illustration, Fig. 6 shows the training samples of the Indian Pines data. Fig.7 (a)-(h) shows the classification results obtained by different methods for the Indian Pines data. Moreover, Table 2 shows all the comparable results of different classifiers. From Table 2, it is obvious that the classifiers with spatial information (Proposed method, NLELM-LBP, SMLR-LBP, KSMLR-LBP) have shown a clear advantage over pixel-only counterpart. NLELM gives the best pixel-only classification results, but the results of NLELM-LBP are not good. This validates that the nonlinear transform will disturb the original salient feature of the original pixels. The reason of bad results of SMLR is that the parameter w in (16) needs to iterate and the outputs of SMLR will disturb the original salient feature of pixels. KSMLR-LBP achieves slightly higher result than SMLR-LBP.

The kernel operation is better than non-kernel operation with the pixel-only classifier. Nevertheless, the result of KSMLR-LBP is still lower than the proposed method. Our proposed spectral-spatial method based on LELM and ILBP achieves the best recognition results. Compared with LELM, NLELM, SMLR, KSMLR, NLELM-LBE, SMLR-LBP, KSMLR-LPB, the proposed framework is higher with 23.99%, 15.41%, 20.32%, 12.82%, 1.49%, 0.7%, 11.85%, respectively. This is due to the usage of the linear transform to keep the original salient features of pixel, and the ILBP to extract the spatial features.

Fig. 8 shows the training samples of Pavia University, and Fig. 9 shows the classification results of

Pavia University and the classification details are reported in Table. 3. It can be seen that the proposed framework achieves the highest accuracy among all the methods. It should be pointed out that, the main obstacle of our method is for the impurity in HSI data sets.

In the last line of Table 2 and Table 3, it reports the average computation times of all the methods on the Indian Pines with 1043 training samples and Pavia University 3921 training samples. It tests for ten Monte Carlo runs, respectively. It is obvious that the classifiers with spectral-spatial information cost more time than the pixel-only counterpart. From the last line of Table 2, we can also see that the proposed method has almost the same computation time as SMLR+LBP for Indian Pines. However, the proposed method achieves higher classification accuracy than SMLR-LBP. The proposed method achieves higher classification accuracy than NLELM-LBP and KSMLR-LBP with much less computation time. From the last line of Table 3, we can get the same conclusion for the Pavia University database. To sum up, the proposed method has achieved higher accuracy than KSMLR-LBP, NLELM-LPB with much less computation time. It is very obviously that the proposed LELM-LBP keeps the salient features of HSI, so it can obtain higher accuracy than other spectral-spatial method with high computational efficiency.

IV. COCLUSION

In this work, we had proposed a new framework for HSI classification using spectral-spatial information with LELM and LBP. The LELM method is used to learn a spectral classifier for the original HSI data and keep the salient features of HSI. The spatial information is modeled based on LBP in order to improve the classification accuracy of HSI. The proposed method keeps the salient feature of HSI in spatial-based classification. Experiment results show the superiority of the proposed method.

In the future work, we will focus on learning the dictionary of each class in the spectral domain for LELM in order to further improve the classification of LELM. Moreover, we will also decrease the time-consuming by resort the extended multi-attribute profiles (EMAPs) [42] method.

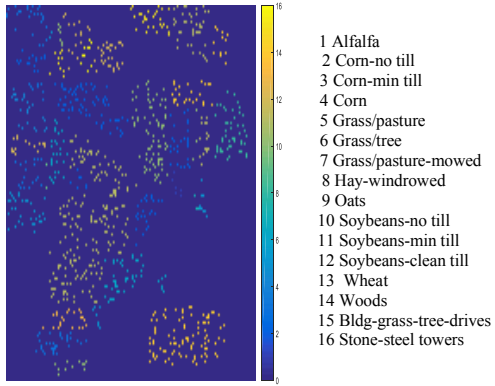


Fig. 6. AVIRIS Indian Pines training maps.

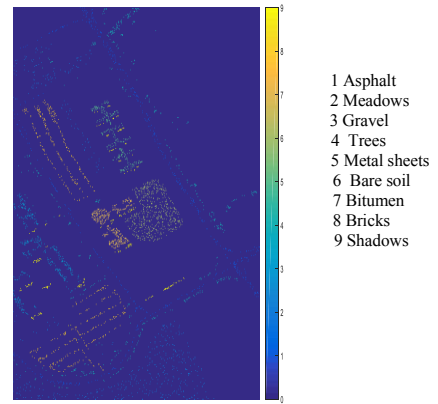


Fig. 8. Pavia University training maps.

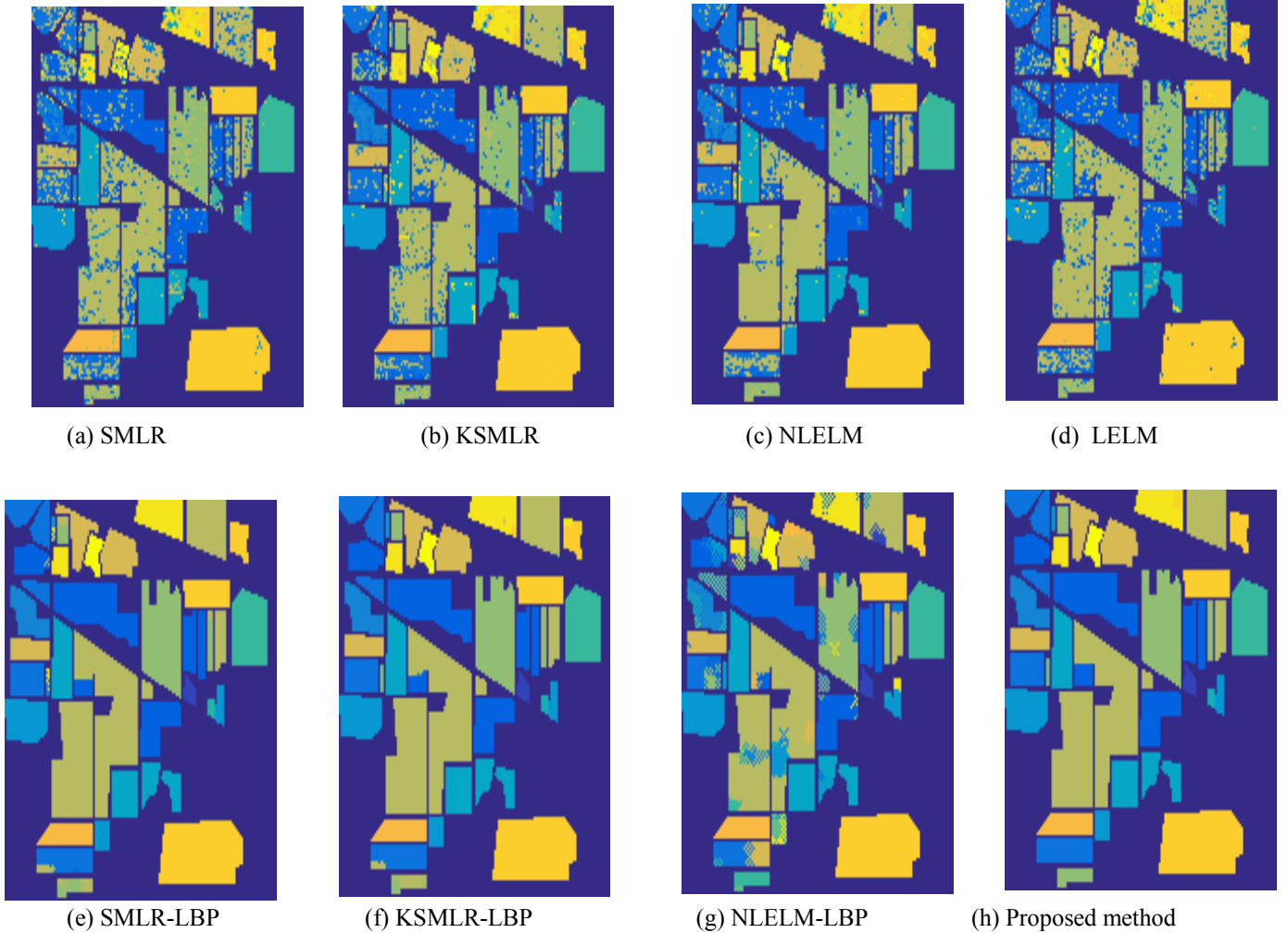


Fig. 7. The overall accuracy of Indian Pines image: (a) SMLR (OA=75.76%); (b) KSMLR (OA=84.34%); (c) NLELM (OA=86.93%); (d) LELM (OA=79.43%); (e) SMLR-LBP (OA=98.26%); (f) KSMLR-LBP (OA=99.05%); (g) NLELM-LBP (OA=87.95%); (h) Proposed method (OA=99.75%).

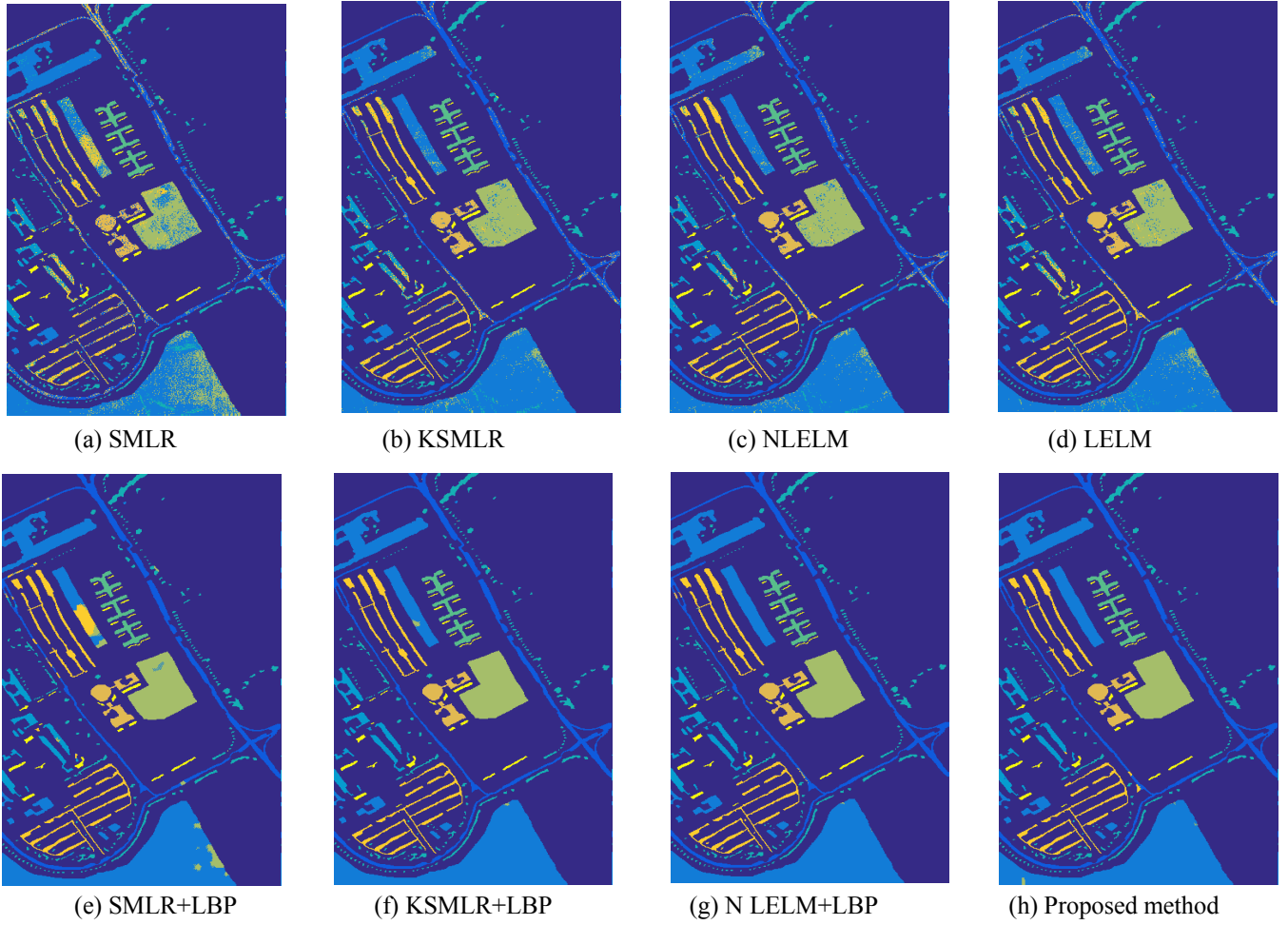


Fig. 9. The overall accuracy of Pavia University image: (a) SMLR (OA=78.78%); (b) KSMLR (OA=93.00%); (c) NLELM (OA=93.94%); (d) LELM (OA=91.23%); (e) SMLR+LBP (OA=95.68%); (f) KSMLR+LBP (OA=99.42%); (g) NLELM+LBP (OA=99.61%); (h) Proposed method (OA=99.82%).

TABLE.2. INDIAN PINES:OVERALL, AVERAGE, AND INDIVIDUAL CLASS ACCYRACY (IN PERCENT) AND K STATISTIC OF DIFFERENT CLSSIFICATION METHODS WITH 10% TRAINING SAMPLES. THE BEST ACCURACY IN EACH ROW IS SHOW IN BOLD.

Class	<i>SMLR</i>	<i>KSMLR</i>	<i>LELM</i>	<i>NLELM</i>	<i>SMLR-LBP</i>	<i>KSMLR-LBP</i>	<i>NLELM-LBP</i>	<i>PROPOSED METHOD</i>
Alfalfa	30.52	74.26	35.37	71.11	97.78	100	90.37	100.00
Corn-no till	75.87	82.49	79.27	85.82	99.02	99.40	85.68	99.68
Corn-min till	51.35	70.86	58.26	72.58	92.55	97.35	68.79	99.22
Corn	37.35	68.68	43.29	69.10	99.27	95.00	77.44	100.00
Grass/pasture	86.82	89.46	89.76	93.64	97.36	98.23	93.64	99.28
Grass/tree	94.28	96.37	96.32	97.39	100.00	100.00	95.70	100.00
Grass/pasture-mowed	6.92	45.00	11.54	70.38	71.92	91.54	45.00	95.38
Hay-windrowed	99.37	98.51	99.57	99.04	100.00	100	98.73	100.00
Oats	5	38.50	11.50	63.50	16.50	100	48.00	100.00
Soybeans-no till	61.03	74.91	66.69	80.79	96.27	96.34	80.74	99.23
Soybeans-min till	74.46	84.51	80.23	87.66	99.96	99.91	90.41	99.93
Soybeans-clean till	68.96	82.20	72.98	84.98	98.50	100	82.85	100.00

Wheat	96.75	99.15	99.39	98.96	100.00	100	98.77	100.00
Woods	95.04	95.20	95.65	96.51	100.00	99.69	97.26	100.00
Bldg-grass-tree-drives	67.13	73.05	64.08	70.45	95.47	99.50	83.53	99.89
Stone-steel towers	69.26	70.32	70.42	77.05	99.58	98.63	98.63	99.89
OA	75.76	84.34	79.43	86.93	98.26	99.05	87.95	99.75
AA	63.66	77.72	67.15	82.44	91.51	98.47	83.47	99.53
k	72.22	82.09	76.38	85.06	98.02	98.92	86.36	99.72
Execution Time (seconds)	0.02	0.41	0.19	0.31	38.74	40.70	39.59	38.95

TABLE.3. PAVIA UNIVERSITY: OVERALL, AVERAGE, AND INDIVIDUAL CLASS ACCYRACY (IN PERCENT) AND k STATISTIC OF DIFFERENT CLSSIFICATION METHODS WITH 10% TRAINING SAMPLES. THE BEST ACCURACY IN EACH ROW IS SHOW IN BOLD.

Class	<i>SMLR</i>	<i>KSMLR</i>	<i>LELM</i>	<i>NLELM</i>	<i>SMLR-LBP</i>	<i>KSMLR-LBP</i>	<i>NLELM-LBP</i>	<i>PROPOSED METHOD</i>
Asphalt	72.27	89.43	85.27	88.82	98.62	99.63	99.49	99.63
Meadows	79.08	94.16	92.17	94.61	93.70	99.34	99.88	99.83
Gravel	71.99	85.08	78.06	87.41	99.14	99.64	99.92	99.83
Trees	94.90	97.92	97.38	98.16	99.27	99.86	98.54	99.64
Metal sheets	99.58	99.34	98.85	99.39	100.00	100.00	100.00	100.00
Bare soil	74.26	94.77	93.90	95.43	99.93	100.00	100.00	100.00
Bitumen	78.66	93.82	93.69	95.34	100.00	100.00	100.00	100.00
Bricks	73.37	87.52	90.05	90.94	99.93	99.63	99.85	100.00
Shadows	96.88	99.61	99.70	99.97	99.89	99.87	94.14	99.89
OA	78.78	93.00	91.23	93.94	96.93	99.59	99.62	99.83
AA	82.33	93.49	92.12	94.56	98.94	99.77	99.09	99.87
k	72.73	90.82	88.54	92.04	95.98	99.46	99.49	99.78
Execution Time (seconds)	0.19	4.40	0.48	3.83	1193.7	1237.1	5288.6	1201.2

ACKNOWLEDGMENT

This work is supported by the National Nature Science Foundation of China (no. 61471132, 61372173), the Training program for outstanding young teachers in higher education institutions of Guangdong Province (no. YQ2015057)

REFERENCES

- [1] M. Sun, D. Zhang, Z. Wang, J. Ren, and J. S. Jin, "Monte Carlo convex hull model for classification of traditional Chinese paintings," *Neurocomputing*, vol. 171, pp. 788-797, 2016.
- [2] F. Melgani, L. Bruzzone, "Classification of hyperspectral remote sensing images with support vector machines," *IEEE Transactions on geoscience and remote sensing*, vol. 42, no. 8, pp. 1778-1790, 2004.
- [3] J. Zabalza, J. Ren, J. Zheng, H. Zhao, C. Qing, Z. Yang, P. Du and S. Marshall, "Novel segmented stacked autoencoder for effective dimensionality reduction and feature extraction in hyperspectral imaging," *Neurocomputing*, vol. 185, pp. 1-10, 2016
- [4] J. Ren, Z. Zabalza, S. Marshall and J. Zheng, "Effective feature extraction and data reduction with hyperspectral imaging in remote sensing," *IEEE Signal Processing Magazine*, vol. 31, no. 4, pp. 149-154, 2014.
- [5] T. Qiao, J. Ren et al, "Effective denoising and classification of hyperspectral images using curvelet transform and singular spectrum analysis," *IEEE Trans. Geoscience and Remote Sensing*, vol. 55, no. 1, pp. 119-133, 2017.
- [6] J. Zabalza, J. Ren, J. Zheng, J. Han, H. Zhao, S. Li, and S. Marshall, "Novel two dimensional singular spectrum analysis for effective feature extraction and data classification in hyperspectral imaging," *IEEE Trans. Geoscience and Remote Sensing*, vol. 55, no. 1, pp. 119-133, 2017.
- [7] T. Qiao, J. Ren, C. Craigie, Z. Zabalza, C. Maltin, S. Marshall, "Singular spectrum analysis for improving hyperspectral imaging based beef eating quality evaluation," *Computers and Electronics in Agriculture*, 2015.
- [8] J. Zabalza, J. Ren, Z. Wang, H. Zhao, J. Wang, and S. Marshall, "Fast implementation of singular spectrum analysis for effective feature extraction in hyperspectral imaging," *IEEE Journal of Selected Topics in Earth Observation and Remote Sensing*, vol. 8, no. 6, pp. 2845-53, 2015.
- [9] J. Zabalza, J. Ren, J. Ren, Z. Liu, and S. Marshall, "Structured covariance principle component analysis for real-time onsite feature extraction and dimensionality reduction in hyperspectral imaging," *Applied Optics*, vol. 53, no. 20, pp. 4440-4449, 2014.
- [10] J. Zabalza, J. Ren, M. Yang, Y. Zhang, J. Wang, S. Marshall, J. Han, "Novel Folded-PCA for Improved Feature Extraction and Data Reduction with Hyperspectral Imaging and SAR in Remote Sensing," *ISPRS Journal of Photogrammetry and Remote Sensing*, vol. 93, no. 7, pp. 112-122, 2014.
- [11] L. Fang, S. Li, W. Duan, J. Ren, J. Atli Benediktsson, "Classification of hyperspectral images by exploiting spectral-spatial information of superpixel via multiple kernels," *IEEE Trans. Geoscience and Remote Sensing*, vol. 53, no. 12, pp. 6663-6674, 2015.
- [12] J. Li, JM. Bioucas-Dias, A. Plaza, "Spectral-spatial classification of hyperspectral data using loopy belief propagation and active learning," *IEEE Transactions on Geoscience and Remote Sensing*, vol. 51, no. 2, pp. 844-856, 2013.
- [13] J. A. Benediktsson, I. Kanellopoulos, "Classification of multisource and hyperspectral data based on decision

fusion,” IEEE Transactions on Geoscience and Remote Sensing, vol. 37, no. 3, pp. 1367-1377, 1993.

[14] A. B. Santos, A. de Albuquerque Araújo, D. Menotti, “Combining multiple classification methods for hyperspectral data interpretation,” IEEE Journal of Selected Topics in Applied Earth Observations and Remote Sensing, vol. 6, no. 3, pp. 1450-1459, 2013.

[15] S. Samiappan, Prasad S, L. M. Bruce, “Non-uniform random feature selection and kernel density scoring with SVM based ensemble classification for hyperspectral image analysis,” IEEE Journal of Selected Topics in Applied Earth Observations and Remote Sensing, vol. 6, no. 2, pp. 792-800, 2013.

[16] B. B. Damodaran, R. R. Nidamanuri, Y. Tarabalka, “Dynamic ensemble selection approach for hyperspectral image classification with joint spectral and spatial information,” IEEE Journal of Selected Topics in Applied Earth Observations and Remote Sensing, vol. 8, no. 6, pp. 2405-2417, 2015.

[17] G. B. Huang, Q. Y. Zhu, and C. K. Siew, “Extreme learning machine: Theory and applications,” Neurocomputing, vol. 70, pp. 489-501, 2006.

[18] Y. Wang, F. Cao, and Y. Yuan, “A study on effectiveness of extreme learning machine,” Neurocomputing, vol. 74, pp. 2483-2490, 2011.

[19] H. J. Rong, Y. S. Ong, A. H. Tan, and Z. Zhu, “A fast pruned-extreme learning machine for classification problem,” Neurocomputing, vol. 72, pp. 359-366, 2008.

[20] G. B. Huang, X. Ding, and H. Zhou, “Optimization method based extreme learning machine for classification,” Neurocomputing, vol. 74, pp. 155-163, 2010.

[21] Samat A, Du P, Liu S, et al. : Ensemble Extreme Learning Machines for Hyperspectral Image Classification. IEEE Journal of Selected Topics in Applied Earth Observations and Remote Sensing, vol. 7, no. 4, pp. 1060-1069, 2014.

[22] G. B. Huang, H Zhou, X. Ding, et al, “Extreme learning machine for regression and multiclass classification.”. IEEE Transactions on Systems, Man, and Cybernetics, Part B (Cybernetics), vol. 42, no. 2, pp. 513-529, 2012.

[23] Z. Bai, G. B. Huang, D. Wang, et al, “Sparse extreme learning machine for classification.”. IEEE transactions on cybernetics, vol.44, no.10, pp. 1858-1870, 2014.

[24] M. Fauvel, Y. Tarabalka, J. A. Benediktsson, et al, “Advances in spectral-spatial classification of hyperspectral images,” Proceedings of the IEEE, vol. 101, no. 3, pp. 652-675, 2013.

[25] Y. Tarabalka, M. Fauvel, Chanussot J, et al, “SVM-and MRF-based method for accurate classification of hyperspectral images,” IEEE Geoscience and Remote Sensing Letters, vol. 7, no. 4, pp. 736-740, 2010.

[26] P. Ghamisi, J. A. Benediktsson, M. O. Ulfarsson, “Spectral-spatial classification of hyperspectral images based on hidden Markov random fields,” IEEE Transactions on Geoscience and Remote Sensing, vol. 52, no. 5, pp. 2565-2574, 2014.

[27] J. S. Yedidia, W. T. Freeman, Y. Weiss, “Understanding belief propagation and its generalizations,” Exploring artificial intelligence in the new millennium, vol. 8, pp. 236-239, 2003.

[28] J. S. Yedidia, W. T. Freeman, Y. Weiss, “Constructing free-energy approximations and generalized belief propagation algorithms,” IEEE Transactions on Information Theory, vol. 51, no. 7, pp. 2282-2312, 2005.

[29] L. Sun, Z. Wu, J. Liu, et al, “Supervised spectral-spatial hyperspectral image classification with weighted Markov random fields,” IEEE Transactions on Geoscience and Remote Sensing, vol. 53, no. 3, pp. 1490-1503, 2015.

[30] J. Li, J. M. Bioucas-Dias, A. Plaza, “Spectral-spatial hyperspectral image segmentation using subspace multinomial logistic regression and Markov random fields,” IEEE Transactions on Geoscience and Remote Sensing, vol. 50, no. 3, pp. 809-823, 2012.

[31] J. Li, J. M. Bioucas-Dias, A. Plaza, “Hyperspectral image segmentation using a new Bayesian approach with active learning,” IEEE Transactions on Geoscience and Remote Sensing, vol. 49, no. 10, pp. 3947-3960, 2011.

[32] B. Krishnapuram, L. Carin, M. A. T. Figueiredo, et al, “Sparse multinomial logistic regression: Fast algorithms and generalization bounds. IEEE transactions on pattern analysis and machine intelligence, vol. 27, no. 6, pp. 957-968, 2005.

[33] S. Kumar, M. Hebert, “Discriminative random fields,” International Journal of Computer Vision, vol. 68, no. 2, pp. 179-201, 2006.

[34] S. Z. Li, “Markov random field modeling in computer vision,” Springer Science & Business Media, 2012.

[35] J. S. Borges, A. R. S. Marçal, J. M. Bioucas-Dias, “Evaluation of Bayesian hyperspectral image segmentation with a discriminative class learning.” Geoscience and Remote Sensing Symposium, 2007. IGARSS 2007. IEEE International. IEEE, pp. 3810-3813, 2003.

[36] J. Li, J. M. Bioucas-Dias, A. Plaza, “Semisupervised hyperspectral image segmentation using multinomial logistic regression with active learning,” IEEE Transactions on Geoscience and Remote Sensing, vol. 48, no. 11, pp. 4085-4098, 2010.

[37] J. Li, J. M. Bioucas-Dias, A. Plaza, “Semi-supervised hyperspectral image classification based on a Markov random field and sparse multinomial logistic regression,” Geoscience and Remote Sensing Symposium, 2009 IEEE International, IGARSS 2009. IEEE, vol. 3, pp. III-817-III-820, 2009.

[38] S. Geman, D. Geman, “Stochastic relaxation, Gibbs distributions, and the Bayesian restoration of images,” IEEE Transactions on pattern analysis and machine intelligence, vol. 6, no. 721-741, 1984.

[39] J. Bioucas-Dias, M. Figueiredo, “Logistic regression via variable splitting and augmented lagrangian tools,” Instituto Superior Técnico, TULisbon, Tech. Rep, 2009.

[40] J. Li, J. M. Bioucas-Dias, A. Plaza, “Hyperspectral image segmentation using a new Bayesian approach with active learning,” IEEE Transactions on Geoscience and Remote Sensing, vol. 49, no. 10, pp. 3947-3960, 2011.

[41] Y. Li, W. Xie, H. Li. “Hyperspectral image reconstruction by deep convolutional neural network for classification,” Pattern Recognition, vol. 63, pp. 371-383, 2017.

[42] M. Dalla Mura, J. A. Benediktsson, B. Waske, et al, “Morphological attribute profiles for the analysis of very high resolution images,” IEEE Transactions on Geoscience and Remote Sensing, vol. 48, no. 10, pp. 3747-3762, 2010.